Nano Energy 96 (2022) 107034

Contents lists available at ScienceDirect

Nano Energy

journal homepage: www.elsevier.com/locate/nanoen

Full paper

Non-adiabatic quantum dynamics of tribovoltaic effects at sliding metal–semiconductor interfaces

Guangming Liu [a,b], Jun Liu [c,d,*], Wenjie Dou [a,b,**]

[a] School of Science, Westlake University, Hangzhou, Zhejiang 310024, China
[b] Institute of Natural Sciences, Westlake Institute for Advanced Study, Hangzhou, Zhejiang 310024, China
[c] Department of Mechanical and Aerospace Engineering, University at Buffalo, The State University of New York, Buffalo, NY 14260, USA
[d] RENEW (Research and Education in Energy, Environment and Water) Institute, University at Buffalo, The State University of New York, Buffalo, NY 14260, USA

ARTICLE INFO

Keywords:
Tribovoltaics
Nonadiabatic dynamics
Electron–phonon couplings
Electron–hole pairs generation
Surface hopping

ABSTRACT

Recent experiments observe electric current generation at sliding metal–semiconductor interfaces. Here, we present a detailed theoretical study on how electric voltage is generated at such a sliding interface. Our study is based on a two-band Anderson–Holstein model, where we solve the coupled electron–phonon dynamics using a surface hopping method. We show that the high local temperature induced by mechanical motion at the interfaces can lead to electron–hole pair generation through electron–phonon couplings. We quantify the efficiency of electron–hole generation as well as electric voltage as a function of local temperatures and semiconductor bandgaps. We find that increasing the local temperatures can lead to higher electron–hole generation and electric voltage. Furthermore, we find that there is a turnover for the electric voltage as a function of the bandgap. Such an observation is in agreement with the experimental results. Our study offers a theoretical framework to understand tribovoltaic effects from a quantum mechanical point of view, and our approach can be used to quantitatively simulate realistic sliding metal–semiconductor junctions.

1. Introduction

When a semiconductor material is involved in a sliding contact, a high direct-current (DC) can be generated, which has been recently observed in various contact material system (e.g. metal/semiconductor [1–3], metal/insulator/semiconductor [3,4], p–n junction [5,6], liquid/semiconductor [7–9]). Such a phenomenon is referred to as "tribovoltaic" effect [10]. Moreover, new multi-physics phenomenon originated from the tribovoltaic effect such as tribo-photovoltaic effect [4,9,11] and tribovoltaic–thermoelectric effect [12] have been found successively in dynamic metal–semiconductor Schottky systems. Although the fundamental mechanism remains unsolved, it is found that the DC current density output of such systems is on the order of 10–100 A/m^2, which is 3–4 orders' higher than which in traditional piezoelectric or triboelectric nanogenerator and thus show a great promise on next-generation mechanical energy harvesting devices for self-powered electronics and Internet of Things (IoTs) sensors [13].

In the past decades, tremendous efforts have been devoted to understanding and quantifying charge transfer during contact. To date, the fundamental physics of triboelectricity remains unsolved [14–16]. The challenge of an explicit understanding of the mechanism resides in the complex multi-scale and multi-physics interaction at a contact interface [17–20]. Frictional energy dissipation in materials may manifest in different ways: heat generation, exo-electron, luminescence, electron–hole generation, surface charges, etc. [21]. In general situation, the majority of frictional energy ends up with heat either through phonon–phonon interaction or relaxation of other electronic excitations. When a Schottky contact consisting of a metal and a semiconductor material is presented however, it is proposed that the input frictional energy may induce a non-adiabatic electronic excitation of energetic carriers, and the generated electron–hole pairs may be non-adiabatic electronic excitation, which ultimately contribute to the DC generation at a sliding Schottky contact [10,22].

The physical essence of charge transfer at the interfaces is the breakdown of Born–Oppenheimer (BO) approximation: In the BO approximation, nuclear motion is assumed to be much slower than electronic motion, such that nuclei move on the adiabatic potential energy surface. Under external stimuli, the accelerated nuclear motion can introduce non-adiabatic electronic transitions between different potential

* Corresponding author.
** Corresponding author at: School of Science, Westlake University, Hangzhou, Zhejiang 310024, China.
E-mail addresses: jliu238@buffalo.edu (J. Liu), douwenjie@westlake.edu.cn (W. Dou).

https://doi.org/10.1016/j.nanoen.2022.107034
Received 9 December 2021; Received in revised form 18 January 2022; Accepted 7 February 2022
Available online 19 February 2022

energy surface near the crossing point such that the BO approximation breaks [23,24]. Nevertheless, a basic understanding of the electronic excitation process in an electro-mechanical coupled system is still missing. In this work, a systematic study on the non-adiabatic electronic excitation at a metal/semiconductor sliding interface using quantum dynamics approach is presented, in an effort to shed light on fundamental process and provide instructional guide for materials design and optimization for future semiconductor-based nanogenerators.

In our previous studies, we have presented a surface hopping dynamics to describe non-adiabatic dynamics near a metal surface [25,26]. In such a dynamical method, we propagate trajectories on different potential energy surfaces describing different charge states. We further introduce stochastic hopping between them indicating charge transfer between these states. Note that, different with Tully's surface hopping method, which is typically used to model non-adiabatic dynamics in solution or in gas phase, our surface hopping is intended to study non-adiabatic dynamics at metal surfaces. Our surface hopping dynamics have been successfully used to describe electron transfer, energy relaxation, current–voltage characteristic near metal surfaces as well as in nano-junctions [27,28].

In this manuscript, we present a two-level Anderson–Holstein model based on electron–phonon couplings to describe the semiconductor-metal interfaces. We use the surface hopping method to describe the non-adiabatic dynamics at such interfaces. Our dynamics indicate that local temperature induced by mechanic motion at the interfaces can lead to electron–hole pair generation through electron–phonon couplings. We can then quantify the generation of the electron and hole population as well as the electric voltage. We find that there is a turnover for the voltage as the function of the bandgap. This finding is in agreement with experimental results. We believe that this article provides atomic insights on how electric current is generated on sliding semiconductor-metal interfaces. We expect that our approach can be used to study realistic sliding metal–semiconductor junctions in the future.

2. Theoretical model

Here, we use a two-level/two-band Anderson–Holstein model to describe semiconductor/metal interfaces. Our total Hamiltonian consists of three parts: $\hat{H}_M$ for the metal, $\hat{H}_S$ for the semiconductor, and $\hat{H}_I$ for the couplings between the metal and the semiconductor, i.e.

$$\hat{H} = \hat{H}_M + \hat{H}_S + \hat{H}_I \tag{1}$$

The metal consists of a manifold of electronic states,

$$\hat{H}_M = \sum_k (\epsilon_k - \mu)\hat{c}_k^+ \hat{c}_k \tag{2}$$

Here $\hat{c}_k^+(\hat{c}_k)$ is the creation (annihilation) operator of an electronic level ϵ_k in the metal. μ is the Fermi energy of the metal (here we set $\mu = 0$). For simplicity, we model the semiconductor with two levels, conduction level/band $E_c(x)$, and valence level/band $E_v(x)$. Here we have a local phonon degrees of freedom (x and p are the position and momentum of the phonon) coupled to the electronic levels. Such that the Hamiltonian for the semiconductor can be written as

$$\hat{H}_S = E_c(x)\hat{d}_c^+\hat{d}_c + E_v(x)\hat{d}_v^+\hat{d}_v + U_0(x) + \frac{p^2}{2m} \tag{3}$$

$U_0(x)$ is the potential for the local phonon mode. $\hat{d}_c^+(\hat{d}_v^+)$ and $\hat{d}_c(\hat{d}_v)$ are the creation and annihilation operator for an electron in the conduction (valence) band of the semiconductor. Below, we will approximate the potential as a harmonic oscillator, $U_0 = \frac{1}{2} m\omega^2 x^2$ (ω is the frequency of the oscillator). The couplings between the metal and levels in the semiconductor are assumed to be bilinear:

$$\hat{H}_I = \sum_k V_{ck}(\hat{c}_k^+\hat{d}_c + \hat{d}_c^+\hat{c}_k) + \sum_k V_{vk}(\hat{c}_k^+\hat{d}_v + \hat{d}_v^+\hat{c}_k) \tag{4}$$

We can define the hybridization functions to characterize the strength of the couplings of electron between the metal and levels in the semiconductor:

$$\Gamma_c = \sum_k |V_{ck}|^2 \delta(\epsilon - \epsilon_k) \tag{5}$$

$$\Gamma_v = \sum_k |V_{vk}|^2 \delta(\epsilon - \epsilon_k) \tag{6}$$

Physically, Γ_c (Γ_v) quantifies the lifetime of an electron in the conduction (valence) band. We further assume that the conduction band and the valence band couple to the local phonon as the following:

$$E_c(x) = g_c x\sqrt{m\omega/\hbar} + E_g/2 \tag{7}$$

$$E_v(x) = g_v x\sqrt{m\omega/\hbar} - E_g/2 \tag{8}$$

Here, $g_c(g_v)$ characterizes the strength of electron–phonon couplings for the conduction (valence) band in the semiconductor. We have assumed that the coupling is linearly proportional to local phonon displacement, which is a typical approximation for the electron–phonon interactions. E_g is the bandgap between the conduction band and valance band.

The above equations conclude our model. The parameters for the model can be obtained from *ab initio* calculations for realistic materials and structures. Our goal is to simulate the electron transfer processes between the conduction/valence band and metal surface. Such processes could lead to electron–hole pair generation in the semiconductor as well as electric voltage. Obviously, solving the real time dynamics will be very difficult. Below, we introduce a classical master equation and surface hopping (SH) method to simulate the dynamical processes.

2.1. Classical master equation

To solve the coupled electron–phonon motion at the interfaces for the two level Anderson–Holstein model introduced above, we explore the classical master equation method. In the limit of weak couplings ($\Gamma < kT$), provided phonon is classical ($\hbar\omega < kT$), we can derive a classical master equation (CME) to describe the dynamics. The exact derivation is similar to the one for one-level Anderson–Holstein model [25,26]. Here we outline the derivation and show the equations of motion.

We start from the Liouville equation for the total system. Under the weak coupling assumption, after tracing over the bath degrees of freedom, we arrive at the quantum master equation for the system only:

$$\partial_t\hat{\rho} = i[\hat{H}_s, \hat{\rho}] - \hat{\hat{\mathcal{L}}}\hat{\rho} \tag{9}$$

Here, $\hat{\rho}$ is density operator for the system. (We have set $\hbar = 1$.) $\hat{\hat{\mathcal{L}}}$ is the Lindblad superoperator coming from the system–bath couplings. Note that, the system includes the electronic states in the semiconductor as well as the phonon degrees of freedom. We further make classical assumption for the phonon using Wigner transformation:

$$\hat{\rho}(x,p) = \int d\Delta x \, \langle x - \Delta x/2|\hat{\rho}|x + \Delta x/2\rangle \exp(ip\Delta x) \tag{10}$$

Here, $\hat{\rho}(x,p)$ can be interpreted as the phase space density for different electronic states. Particularly, we have ρ_0, ρ_v, ρ_c, ρ_{vc} to denote the phase space densities with empty electron, one electron in the valance band, one electron in the conduction band, and two electrons, respectively. The equations of motion for these densities are:

$$\begin{aligned}\partial_t\rho_0 &= \frac{p}{m}\partial_x\rho_0 - \partial_x U_0\partial_p\rho_0 - (\Gamma_c f(E_c) + \Gamma_v f(E_v))\rho_0 + \Gamma_c f(-E_c)\rho_c \\ &\quad + \Gamma_v f(-E_v)\rho_v \end{aligned} \tag{11}$$

$$\begin{aligned}\partial_t\rho_v &= \frac{p}{m}\partial_x\rho_v - \partial_x U_1\partial_p\rho_v + \Gamma_v f(E_v)\rho_0 - (\Gamma_c f(E_c) + \Gamma_v f(-E_v))\rho_v \\ &\quad + \Gamma_c f(-E_c)\rho_{vc} \end{aligned} \tag{12}$$

$$\begin{aligned}\partial_t\rho_c &= \frac{p}{m}\partial_x\rho_c - \partial_x U_2\partial_p\rho_c + \Gamma_c f(E_c)\rho_0 - (\Gamma_c f(-E_c) + \Gamma_v f(E_v))\rho_c \\ &\quad + \Gamma_v f(-E_v)\rho_{vc} \end{aligned} \tag{13}$$

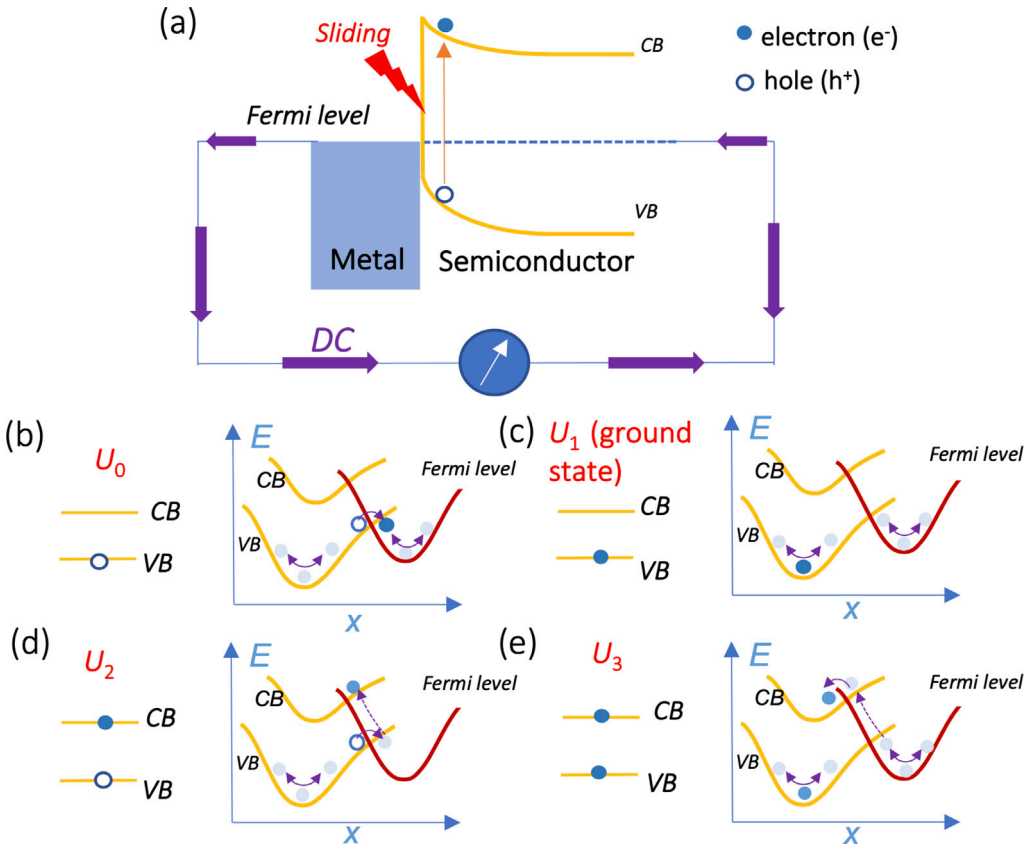

Fig. 1. (a) Schematic band diagram of a metal–semiconductor dynamic contact (CB, conduction band; VB, valence band). Schematics of four energy states: (b) U_0, one hole on the VB. Such state can be arrived from the ground state (U_1) by transferring one electron from the VB of the semiconductor to the metal. (c) $U_1 = U_0 + E_v$, one electron on the VB, i.e. the ground state. (d) $U_2 = U_0 + E_c$, one electron on the CB and one hole on the VB. Such state can be arrived from the ground state by transferring one electron from the VB of the semiconductor to the metal, then to the CB of the semiconductor sequentially. (e) $U_3 = U_0 + E_v + E_c$, one electron on the VB and one electron on the CB. Such state can be arrived from the ground state by transferring one electron from the metal to the CB of the semiconductor. x is the reaction coordinate (phonon degree of freedom). Non-adiabatic charge transfer between the four states occurs via electron–phonon couplings.

$$\partial_t \rho_{vc} = \frac{p}{m}\partial_x \rho_{vc} - \partial_x U_3 \partial_p \rho_{vc} + \Gamma_c f(E_c)\rho_c + \Gamma_v f(E_v)\rho_v - (\Gamma_c f(-E_c) + \Gamma_v f(-E_v))\rho_{vc} \tag{14}$$

Here, $f(x) = 1/(e^{(x-\mu)/kT} + 1)$ is the Fermi function. $U_1 = U_0 + E_v$, $U_2 = U_0 + E_c$, and $U_3 = U_0 + E_c + E_v$ correspond to the potential energy surfaces (PESs) for one electron in the valance band, one electron in the conduction band, and two electrons, respectively. We note that, the densities follow the classical motion on the corresponding potential energy surfaces with transitions between different electronic states. The hopping rates are proportional to the hybridization function (Γ_c or Γ_v) as well as the Fermi functions. In Fig. 1, we show the four electronic states for the semiconductor with two levels near a continuum of electronic states (metal surface). We refer to the state with one electron on the valence band (U_1) as our ground state. The other states can be arrived from the ground state by transferring electrons between the metal and the semiconductors. In particular, the state with no electron is referred to as one hole state (U_0), and the state with one electron on the conduction band is referred to as electron–hole pair state (U_2).

In Fig. 2, we plot the potential energy surfaces (PESs) for different electronic states. Notice that there are several crossings between the PESs when the bandgap E_g is small. When the bandgap is large, the crossing can only happen at very high energies. At the crossing points, the hopping happens most frequently. At very low nuclear energy, the electrons will likely remain on the ground state. With higher nuclear energy, there will be more transitions on the excited states. Below, we will use a surface hopping algorithm to propagate the equation of motion and analyze non-adiabatic electron transfer between semiconductor and metal surfaces.

3. Numerical results

We now use the surface hopping algorithm to solve the CME dynamics. In the surface hopping method, we use a swarm of trajectories to represent nuclear densities. We evolve trajectories on the active potential energy surfaces (PESs), and we introduce hopping between the PESs. At each time step, we generate a random number uniformly distributed from 0 to 1; we then compare the random number to hopping rate times dt (dt is the time interval). A hopping to a different potential energy surface occurs when the random number is smaller than the hopping rate times dt; otherwise, the trajectory remains on the original PES. In Fig. 3, we show hopping events between the four potential energy surfaces of one trajectory in real time. Note that there are 8 possible transition events between the 4 PESs (see Eqs. (11)–(14)). The red dots denote these 8 possible hopping events.

In a sliding metal–semiconductor junction, the mechanical motion could induce phonon excitation, especially at the local contact asperities, which have a typical size of 10–100 nm. The single asperities at contact interfaces experience a large local pressure at GPa level and a local contact temperature T as high as 1000 K [29,30]. Such excited phonon motion could then introduce electron–hole pairs as well as voltage generation through electron–phonon couplings. To mimic a such process, we initialize all trajectories on the ground state (one electron in the valance band, with PES $U_1 = U_0 + E_v$), where the momentums and positions of these trajectories satisfy a Boltzmann distribution at a given initial phonon temperature T_i,

$$\rho_v(x,p) = \frac{\omega}{2\pi k T_i}\exp\left(-\frac{1}{kT_i}\left(\frac{p^2}{2m} + \frac{1}{2}m\omega^2(x-x_0)^2\right)\right) \tag{15}$$

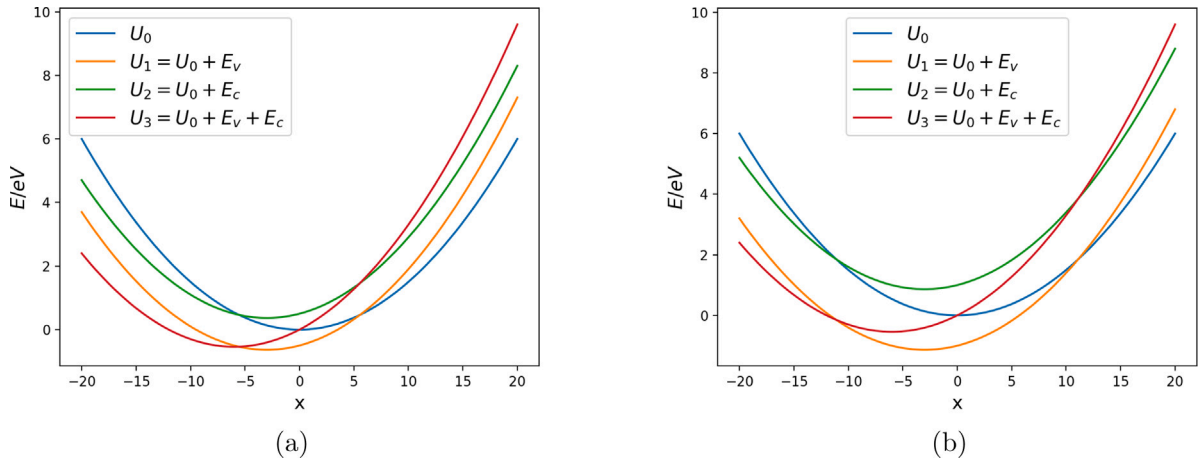

Fig. 2. Potential energy surfaces for different charge states: U_0, no electron in either conduction or valance band; $U_1 = U_0 + E_v$, one electron in the valence band; $U_2 = U_0 + E_c$, one electron in the conduction band; and $U_3 = U_0 + E_v + E_c$ two electrons in the conduction and valance band. Parameters: (a) $\hbar\omega = 0.03$ eV, $g_c = g_v = 0.09$ eV, $E_g = 1$ eV (b) $\hbar\omega = 0.03$ eV, $g_c = g_v = 0.09$ eV, $E_g = 2$ eV. Here, we have set $m = \frac{\hbar}{2\omega}$.

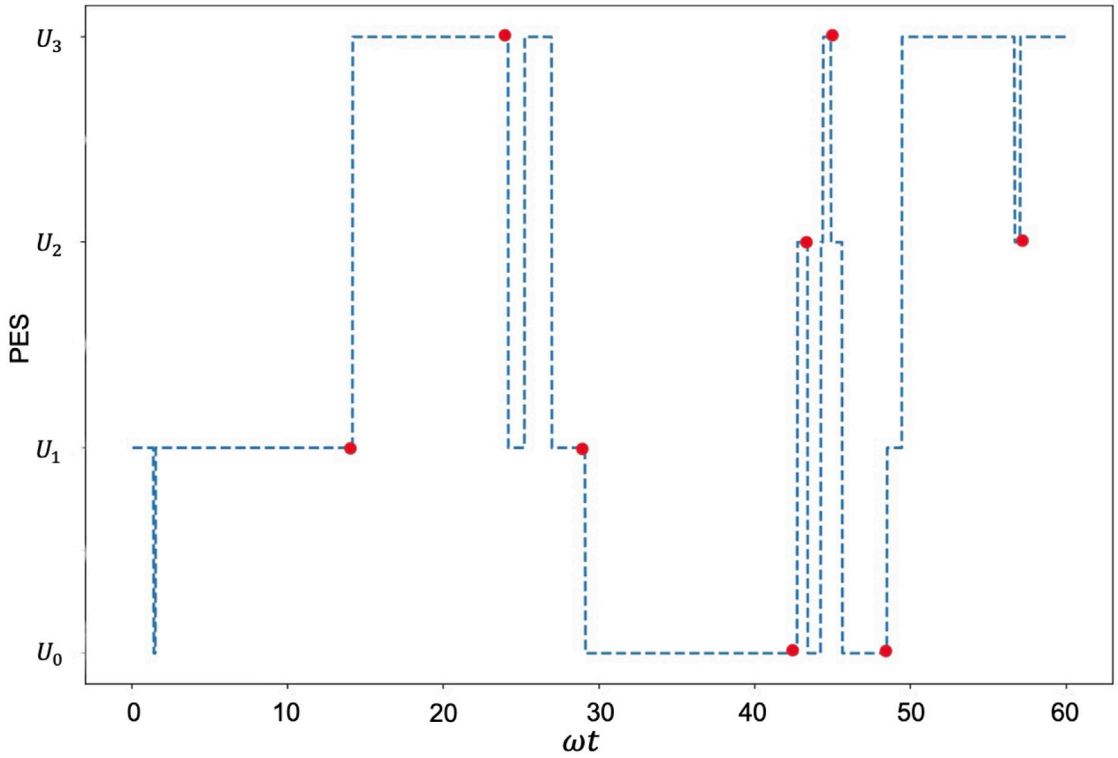

Fig. 3. Hopping events between the four potential energy surfaces of one trajectory. According to Eqs. (11)–(14), each state can hop to two other states (e.g. $U_0 \to U_1$, $U_0 \to U_2$), hence 8 possible hopping events in total. The red dots denote these 8 possible hopping events.

$$\rho_0 = \rho_c = \rho_{vc} = 0 \tag{16}$$

Here, $x_0 = -\sqrt{\frac{\hbar}{m\omega}}\frac{g_v}{\hbar\omega}$ is the position of lowest energy on the ground state. We then evolve our equation of motion to see how phonon energy relaxes and how electron–hole pairs are generated as a function of time. In our simulation, we use 4th order Runge–Kutta to propagate the dynamics. Unless otherwise stated, we use 10000 trajectories for our SH simulations.

3.1. Phonon relaxation

We first look at the phonon relaxation at the interfaces. In Fig. 4(a), we initialize our phase space density on the ground state with different phonon temperatures T_i, and we plot average kinetic energy as a function of time. Here, we fix the temperature of the metal (electron bath, $kT = 0.05$ eV), which only appears in the equation of motion through the Fermi distribution in the hopping rates. we note that, the kinetic energy of the phonon will reach to the same steady state, with the average kinetic energy being half kT, i.e. the temperature of the metal, regardless of the initial conditions. In fact, we can verify that, the steady state nuclear distribution will obey a Boltzmann distribution with the same temperature of the metal (see Refs. [25,26]). Physically, this observation indicates that when the phonon degrees of freedom interact with a manifold of electronic states long enough, the phonon will reach to an equilibrium distribution with the same temperature as the electronic bath. Note also that, the relaxation rate is independent of the initial kinetic energy. As shown in Ref. [27,31], the relaxation rate strongly depends on the electron–phonon couplings g_c (or g_v), the

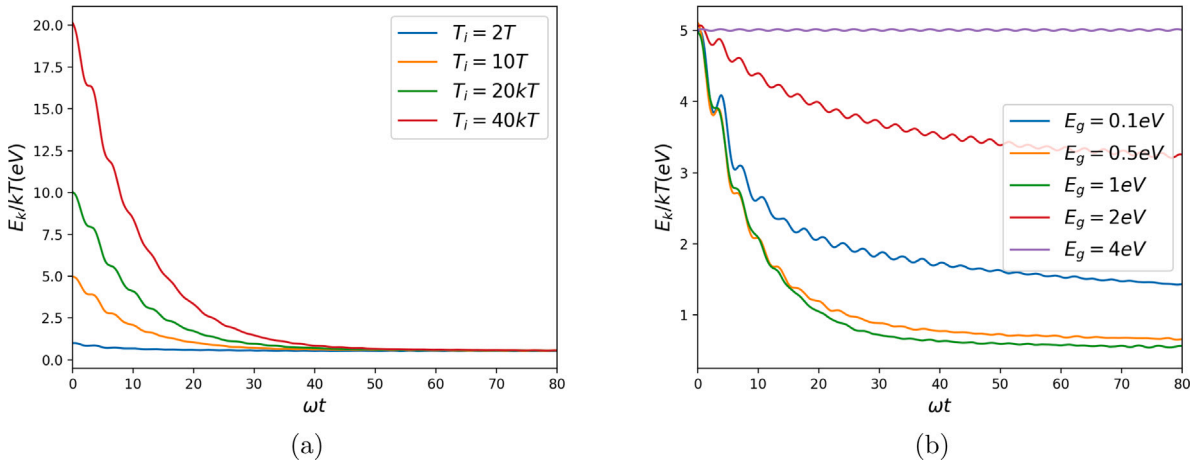

Fig. 4. Phonon relaxation: $\hbar\omega = 0.03$ eV, $g_c = g_v = 0.09$ eV, $kT = 0.05$ eV, $\Gamma_c = \Gamma_v = 0.02$ eV. (a) Phonon Relaxation with different initial conditions, T_i represents the temperature at which the oscillator is initialized. (b) Phonon relaxation with different bandgaps, E_g (eV).

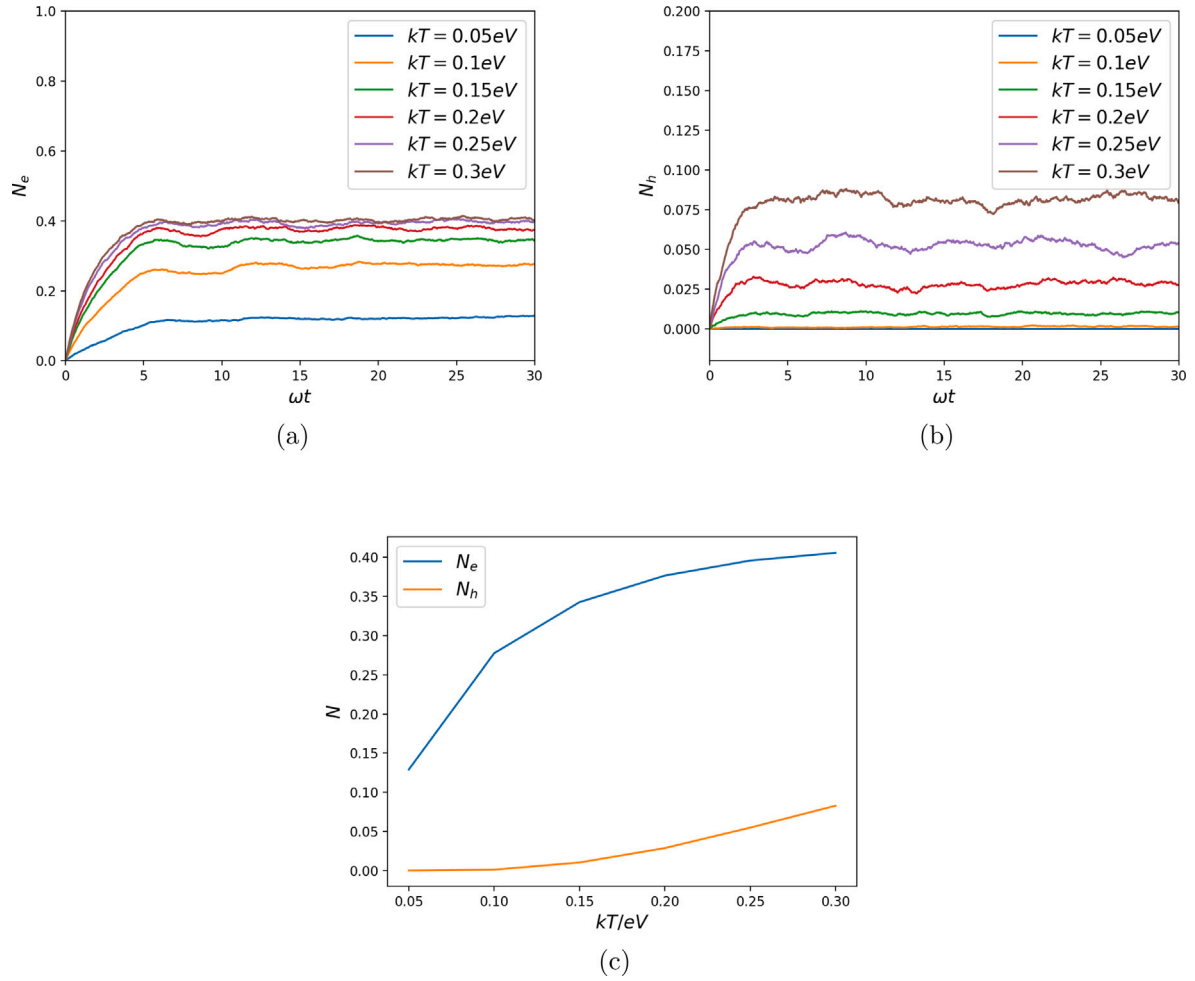

Fig. 5. Electron and hole populations at different local temperatures. (a) Electron population as a function of time. (b) Hole population as a function of time. (c) Steady state population of electrons and holes as a function of local temperatures. Parameters: $\hbar\omega = 0.03$ eV, $g_c = g_v = 0.09$ eV, $E_g = 1$ eV, $\Gamma_c = \Gamma_v = 0.02$ eV.

timescales of electronic motion Γ_c and/or Γ_v, and the timescale of the nuclear motion $\hbar\omega$.

In Fig. 4(b), we plot the phonon relaxation for different band gaps E_g. We have fixed the initial phonon temperature, $T_i = 10T$. Here, we observe a turnover of the relaxation timescales for different bandgaps. (1) For the case where the bandgap $E_g > 1$ eV, the relaxation takes longer for larger bandgaps. In fact, for the bandgap as large as $E_g = 4$ eV, we do not see energy relaxation at all. This is because when the band gap is large enough, the crossing between PESs will only occur at very large potentials (see Fig. 2), such that hopping events are very rare, which results in little or no energy relaxation. (2) For the cases where the bandgap $E_g < 1$ eV, the relaxation timescales could also be

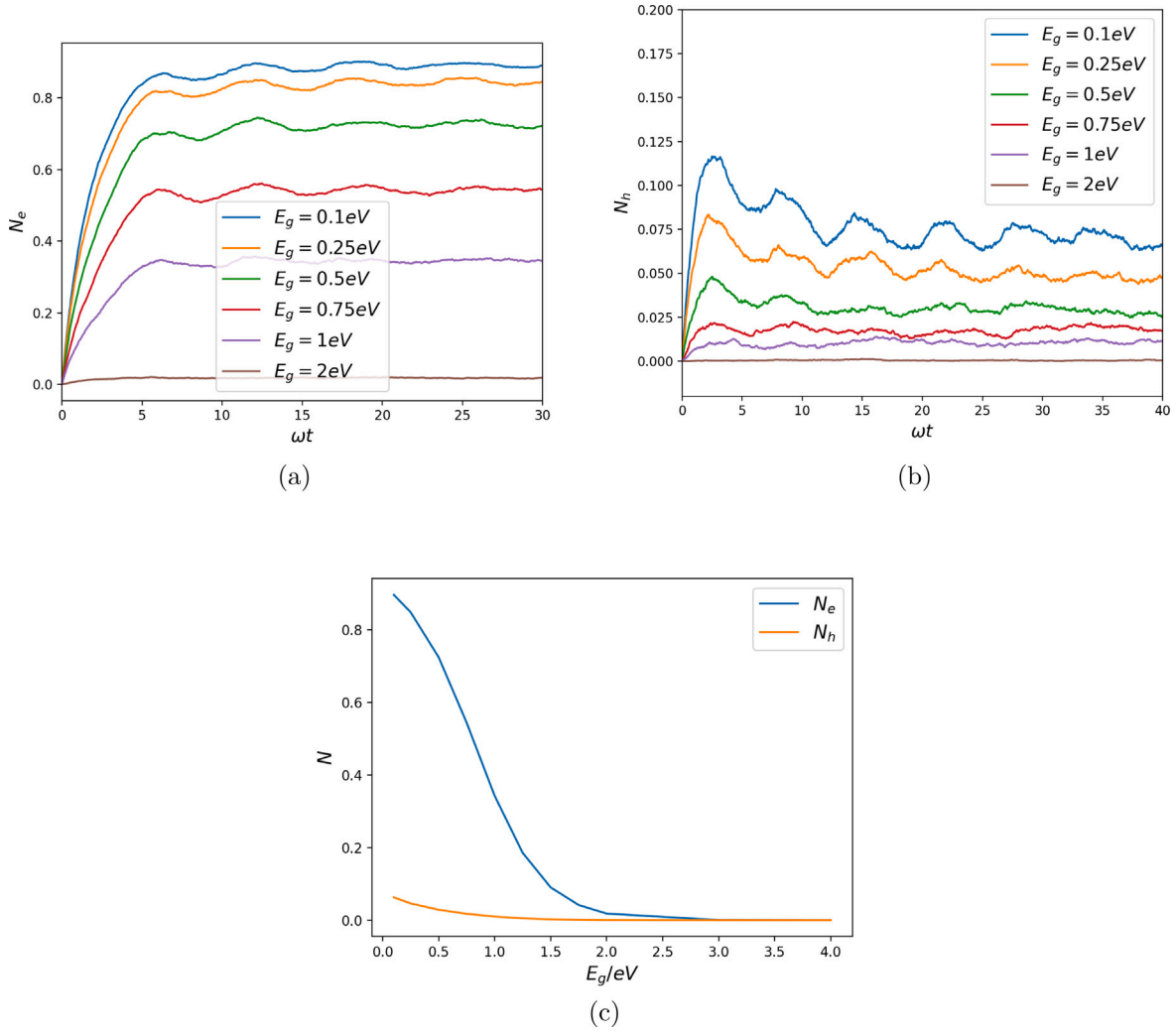

Fig. 6. Electron and hole populations for different bandgaps (eV). (a) Electron population as a function of time. (b) Hole population as a function of time. (c) Steady state electron and hole populations as a function of bandgap. Parameters: $\hbar\omega = 0.03$ eV, $g_c = g_v = 0.09$ eV, $kT = 0.15$ eV.

larger for smaller bandgaps. This is due to the fact that when hopping occurs, the energy loss is small if the bandgaps are small. The relaxation timescale is a result of two competing effects: the frequency of hopping and energy loss when hopping events occur. Increasing the bandgap will reduce the frequency of hopping, but increase energy loss when hopping events occur.

3.2. Electron and hole populations

In a sliding metal–semiconductor interfaces, the open-circuit voltage (V_{oc}) generation (tribovoltaic potential difference between the metal and the semiconductor) is associated with the electron–hole (e–h) pair generation in a mechanically excited system [10,22]. To quantify the electron–hole (e–h) pair generation, we define the electron population on the conduction band N_e as well as the hole population on the valence band N_h as follows:

$$N_e = \int \big(\rho_c(x,p) + \rho_{vc}(x,p)\big)dxdp, \tag{17}$$

$$N_h = \int \big(\rho_0(x,p) + \rho_c(x,p)\big)dxdp \tag{18}$$

Here again, $\rho_c(x,p)$ is the phase space density for the one electron and one hole state, $\rho_{vc}(x,p)$ is the density for two electron states, and $\rho_0(x,p)$ is the density for one hole state (see Fig. 2). N_e and N_h are dimensionless in our definition.

In Figs. 5(a) and 5(b), we plot hole and electron populations at different temperatures as a function of time. Here the initial phonon temperature T_i is set to be equal to the temperature of the electron or the local temperature of the asperities T. We further vary the contact temperature at the single asperities depending on mechanical motion parameters (e.g. pressure and speed) at a sliding metal–semiconductor junction. We find that the timescales for electron and hole generation are roughly the same. In general, the steady state electron generation is larger than the hole generation. The difference in electron and hole populations is very related to the potential energy shifts (e.g. electron–phonon couplings, g_c and g_v) as well as temperature. When the local temperature is small enough ($\lesssim 0.1$ eV), there will be nearly no hole generation. This can be seen from Fig. 2(a): U_3 is the lowest excited states, whereas U_0 and U_2 are excited states with higher energies. At small local temperatures, there will be little distribution on potential surface U_0 and U_2, and most of the excited states is on potential surface U_3.

To further illustrate the temperature effects, in Fig. 5(c), we further plot electron and hole populations as a function of temperature at the steady states. Note that both electron and hole populations increase with temperature. This observation is in agreement with experimental

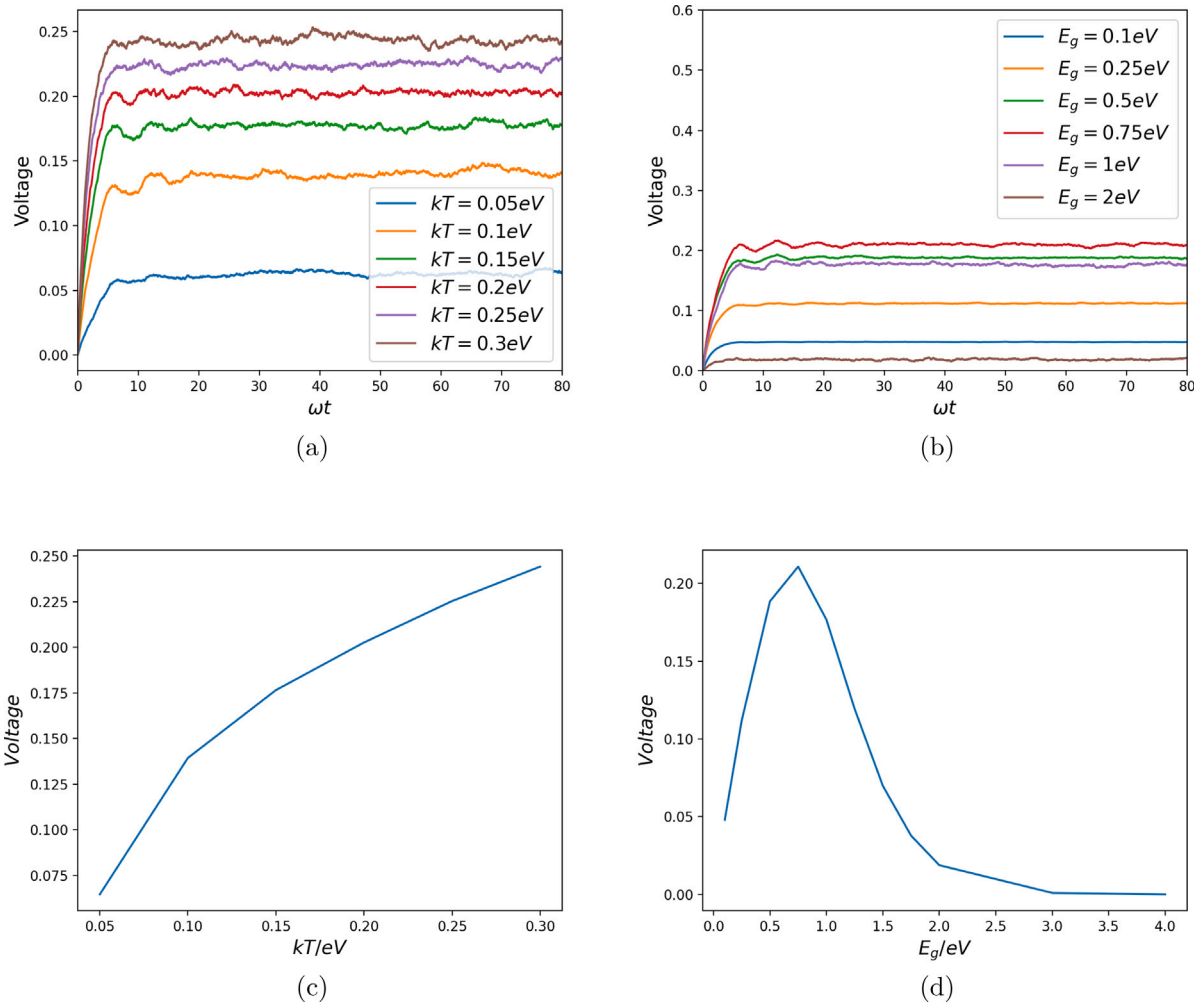

Fig. 7. Average voltage (V_{oc}) for different local temperatures and bandgaps. (a) V_{oc} as a function of time for different temperatures, $E_g = 1$ eV. (b) V_{oc} as a function of time for different bandgaps, $kT = 0.15$ eV. (c) Steady state V_{oc} as a function of temperature, $E_g = 1$ eV. (d) Steady state V_{oc} as a function of bandgap, $kT = 0.15$ eV. Other parameters: $\hbar\omega = 0.03$ eV, $g_c = g_v = 0.09$ eV.

results. With faster mechanical motion and higher pressure at the interfaces, the temperature of local asperities is larger, such that more electron–hole pairs are generated at the interfaces. Again, we see the asymmetry of electron and hole generations at given temperature. We hope future experimental results can justify our simulation.

We now study the effects of bandgap on the electron and hole generations. In Figs. 6(a) and 6(b), we plot hole and electron populations at different bandgaps as a function of time. Notice that the timescales for electron and hole generations strongly depends on bandgaps. As indicated before (see Section 3.1), the bandgap strongly affects the hopping rates, which in turn determines the timescale for population relaxation. Note that, for certain bandgaps, the timescales for the hole generation can be much longer than the electron. In Fig. 6(c), we plot the steady state electron and hole populations as a function of bandgaps. We see that the steady state electron and hole population decrease with the bandgap. Obviously, with larger bandgaps, the chance of occupying excited state decreases, such that there will be less electron and hole generations. In fact, from our calculation, we see that there is almost no electron and hole generation for the bandgap as large as 3 eV. Such a fact will show their signature in the voltage generation as depicted below.

3.3. Voltage generation

With the definition of the electron and hole generations in Eqs. (17) and (18), it is natural to define the open-circuit voltage (V_{oc}) as

$$V_{oc} = \frac{1}{e}\int \Big(\rho_0(x,p)\times\frac{E_g}{2} + \rho_v(x,p)\times 0 + \rho_c(x,p)\times E_g + \rho_{vc}(x,p) \times\frac{E_g}{2}\Big)\, dxdp = \frac{1}{2e}E_g(N_e+N_h) \tag{19}$$

Here e is the elementary charge. N_e and N_h are the populations of excited electron and hole, respectively. See Eqs. (17) and (18). (ρ_0, ρ_v, ρ_c, and ρ_{vc} are the probability densities for the four corresponding states in phase space. Since we have set the Fermi level in the middle of the bandgap, we expect that one excited electron or one hole will contribute to $E_g/2$ voltage relative to the metal. Hence, $E_g/2$ times the electron plus hole populations gives the total voltage.

In Fig. 7(a), we plot voltage as a function of time for different temperatures. Note that at longer time, the voltages reach to stationary values. To further illustrate the effects of the temperature, we plot the steady state voltages as a function of the temperature in Fig. 7(c). Here we see that the steady state voltage increases with the temperature. This result is consistent with the observation in Fig. 5(c), where both N_e and N_h increase with temperature. In general, larger local temperature

will lead to higher voltage generation. Again, this is in agreement with the experimental results [32].

In Fig. 7(b), we plot V_{oc} as a function of time for different bandgaps (E_g). Notice that for smaller bandgaps (< 0.75 eV), the steady state voltage increase with the bandgap; Whereas for larger bandgaps (> 0.75 eV) the steady state voltage decreases with bandgap. This is further shown in Fig. 7(d), where we clearly see a turnover for the voltage as a function of the bandgaps. The turning point is around 0.75 eV for the bandgaps. This turnover is a result of two competing factors: the electron–hole populations as well as the bandgaps. See the definition of voltage in Eq. (19). With small bandgap, there is little voltage generation. Increasing the bandgap will lead to less electron and hole generations. When the bandgap is large enough, there will be no electron and hole generations, hence no voltage generation. Such a turnover is being observed in experiments [32]. We hope to quantify this turnover more precisely for realistic systems in the future study.

4. Conclusions

We have offered a quantum mechanical perspective of the tribovoltaic effects at sliding metal–semiconductor interfaces. We have introduced a two-level Anderson–Holstein model to describe non-adiabatic electron and energy transfer at the interfaces. Furthermore, we have used the classical master equation (CME) as well as the surface hopping algorithm to model the coupled electron–phonon dynamics. Using such a dynamical method, we can quantify the electron–hole pair generations as well as voltage generations. We find that, the electron and hole populations increase with local temperature, but decrease with the bandgap. However, there is a turnover for the voltage generation as a function of the bandgaps. This finding is strongly supported by the experimental results. We believe this work presents an atomic description of tribovoltaic effects. Future work must apply our approach to realistic systems for better design and control of sliding metal–semiconductor junctions. Extension of the current method for doped materials will also be studied in the future.

CRediT authorship contribution statement

Guangming Liu: Performed the calculations, Data analysis, Writing – original draft. **Jun Liu:** Designed the research, Data analysis, Writing – original draft. **Wenjie Dou:** Designed the research, Data analysis, Writing – original draft.

Declaration of competing interest

The authors declare that they have no known competing financial interests or personal relationships that could have appeared to influence the work reported in this paper.

Data availability

The data that support the findings of this study are available from the corresponding author upon reasonable request

Acknowledgments

WD acknowledges the startup funding from Westlake University, China.

References

[1] J. Liu, A. Goswami, K. Jiang, F. Khan, S. Kim, R. McGee, Z. Li, Z. Hu, J. Lee, T. Thundat, Direct-current triboelectricity generation by a sliding Schottky nanocontact on MoS2 multilayers, Nature Nanotechnol. 13 (2018) 112–116.
[2] J. Liu, F. Liu, R. Bao, K. Jiang, F. Khan, Z. Li, H. Peng, J. Chen, A. Alodhayb, T. Thundat, Scaled-up direct-current generation in MoS2 multilayer-based moving heterojunctions, ACS Appl. Mater. Interfaces 11 (2019) 35404–35409.
[3] J. Liu, M. Miao, K. Jiang, F. Khan, A. Goswami, R. McGee, Z. Li, L. Nguyen, Z. Hu, J. Lee, et al., Sustained electron tunneling at unbiased metal–insulator-semiconductor triboelectric contacts, Nano Energy 48 (2018) 320–326.
[4] Z. Hao, T. Jiang, Y. Lu, S. Feng, R. Shen, T. Yao, Y. Yan, Y.M. Yang, Y. Lu, S. Lin, Co-harvesting light and mechanical energy based on dynamic metal/perovskite Schottky junction, Matter 1 (2019) 639–649.
[5] R. Xu, Q. Zhang, J.Y. Wang, D. Liu, J. Wang, Z.L. Wang, Direct current triboelectric cell by sliding an n-type semiconductor on a p-type semiconductor, Nano Energy 66 (2019) 104185.
[6] M. Zheng, S. Lin, L. Xu, L. Zhu, Z.L. Wang, Scanning probing of the tribovoltaic effect at the sliding interface of two semiconductors, Adv. Mater. 32 (2020) 2000928.
[7] S. Lin, X. Chen, Z.L. Wang, The tribovoltaic effect and electron transfer at a liquid-semiconductor interface, Nano Energy 76 (2020) 105070.
[8] Y. Lu, Q. Gao, X. Yu, H. Zheng, R. Shen, Z. Hao, Y. Yan, P. Zhang, Y. Wen, G. Yang, et al., Interfacial built-in electric field-driven direct current generator based on dynamic silicon homojunction, Research 2020 (2020).
[9] M. Zheng, S. Lin, Z. Tang, Y. Feng, Z.L. Wang, Photovoltaic effect and tribovoltaic effect at liquid-semiconductor interface, Nano Energy 83 (2021) 105810.
[10] Z. Zhang, D. Jiang, J. Zhao, G. Liu, T. Bu, C. Zhang, Z.L. Wang, Tribovoltaic effect on metal–semiconductor interface for direct-current low-impedance triboelectric nanogenerators, Adv. Energy Mater. 10 (2020) 1903713.
[11] J. Liu, Y. Zhang, J. Chen, R. Bao, K. Jiang, F. Khan, A. Goswami, Z. Li, F. Liu, K. Feng, et al., Separation and quantum tunneling of photo-generated carriers using a tribo-induced field, Matter 1 (2019) 650–660.
[12] Z. Zhang, T. He, J. Zhao, G. Liu, Z. Wang, C. Zhang, Tribo-thermoelectric and tribovoltaic coupling effect at metal–semiconductor interface, Mater. Today Phys. 16 (2021) 100295.
[13] R. Yang, R. Xu, W. Dou, M. Benner, Q. Zhang, J. Liu, Semiconductor-based dynamic heterojunctions as an emerging strategy for high direct-current mechanical energy harvesting, Nano Energy (2021) 105849.
[14] D.J. Lacks, T. Shinbrot, Long-standing and unresolved issues in triboelectric charging, Nature Rev. Chem. 3 (2019) 465–476.
[15] J. Lowell, A. Rose-Innes, Contact electrification, Adv. Phys. 29 (1980) 947–1023.
[16] Z.L. Wang, A.C. Wang, On the origin of contact-electrification, Mater. Today 30 (2019) 34–51.
[17] R. Alicki, A. Jenkins, Quantum theory of triboelectricity, Phys. Rev. Lett. 125 (2020) 186101.
[18] M. Willatzen, L.C. Lew Yan Voon, Z.L. Wang, Quantum theory of contact electrification for fluids and solids, Adv. Funct. Mater. 30 (2020) 1910461.
[19] A.C. Antony, D. Thelen, N. Zhelev, K. Adib, R.G. Manley, Electronic charge transfer during metal/SiO2 contact: Insight from density functional theory, J. Appl. Phys. 129 (2021) 065304.
[20] K.M. Abdelaziz, J. Chen, T.J. Hieber, Z.C. Leseman, Atomistic field theory for contact electrification of dielectrics, J. Electrost. 96 (2018) 10–15.
[21] J.Y. Park, M. Salmeron, Fundamental aspects of energy dissipation in friction, Chem. Rev. 114 (2014) 677–711.
[22] J. Liu, K. Jiang, L. Nguyen, Z. Li, T. Thundat, Interfacial friction-induced electronic excitation mechanism for tribo-tunneling current generation, Mater. Horiz. 6 (2019) 1020–1026.
[23] W. Dou, J.E. Subotnik, Nonadiabatic molecular dynamics at metal surfaces, J. Phys. Chem. A 124 (2020) 757–771.
[24] H. Nienhaus, Electronic excitations by chemical reactions on metal surfaces, Surf. Sci. Rep. 45 (2002) 1–78.
[25] W. Dou, A. Nitzan, J.E. Subotnik, Surface hopping with a manifold of electronic states. II. Application to the many-body anderson–holstein model, J. Chem. Phys. 142 (2015) 084110.
[26] W. Dou, A. Nitzan, J.E. Subotnik, Surface hopping with a manifold of electronic states. III. Transients, broadening, and the marcus picture, J. Chem. Phys. 142 (2015) 234106.
[27] W. Ouyang, W. Dou, A. Jain, J.E. Subotnik, Dynamics of barrier crossings for the generalized Anderson–Holstein model: Beyond electronic friction and conventional surface hopping, J. Chem. Theory Comput. 12 (2016) 4178–4183.
[28] W. Dou, C. Schinabeck, M. Thoss, J.E. Subotnik, A broadened classical master equation approach for treating electron-nuclear coupling in non-equilibrium transport, J. Chem. Phys. 148 (2018) 102317.

[29] F.E. Kennedy, Frictional heating and contact temperatures, in: Modern Tribology Handbook, vol. 1, 2001, pp. 235–272.
[30] F. Kennedy, Frictional heating and contact temperatures—chapter 6, in: Modern Tribology HandBook, 2020, p. 1.
[31] W. Dou, A. Nitzan, J.E. Subotnik, Frictional effects near a metal surface, J. Chem. Phys. 143 (2015) 054103.
[32] M. Benner, R. Yang, L. Lin, M. Liu, H. Li, J. Liu, Mechanism of in-plane and out-of-plane tribovoltaic direct-current transport with a metal/oxide/metal dynamic heterojunction, ACS Appl. Mater. Interfaces (2022) PMID: 34990542.